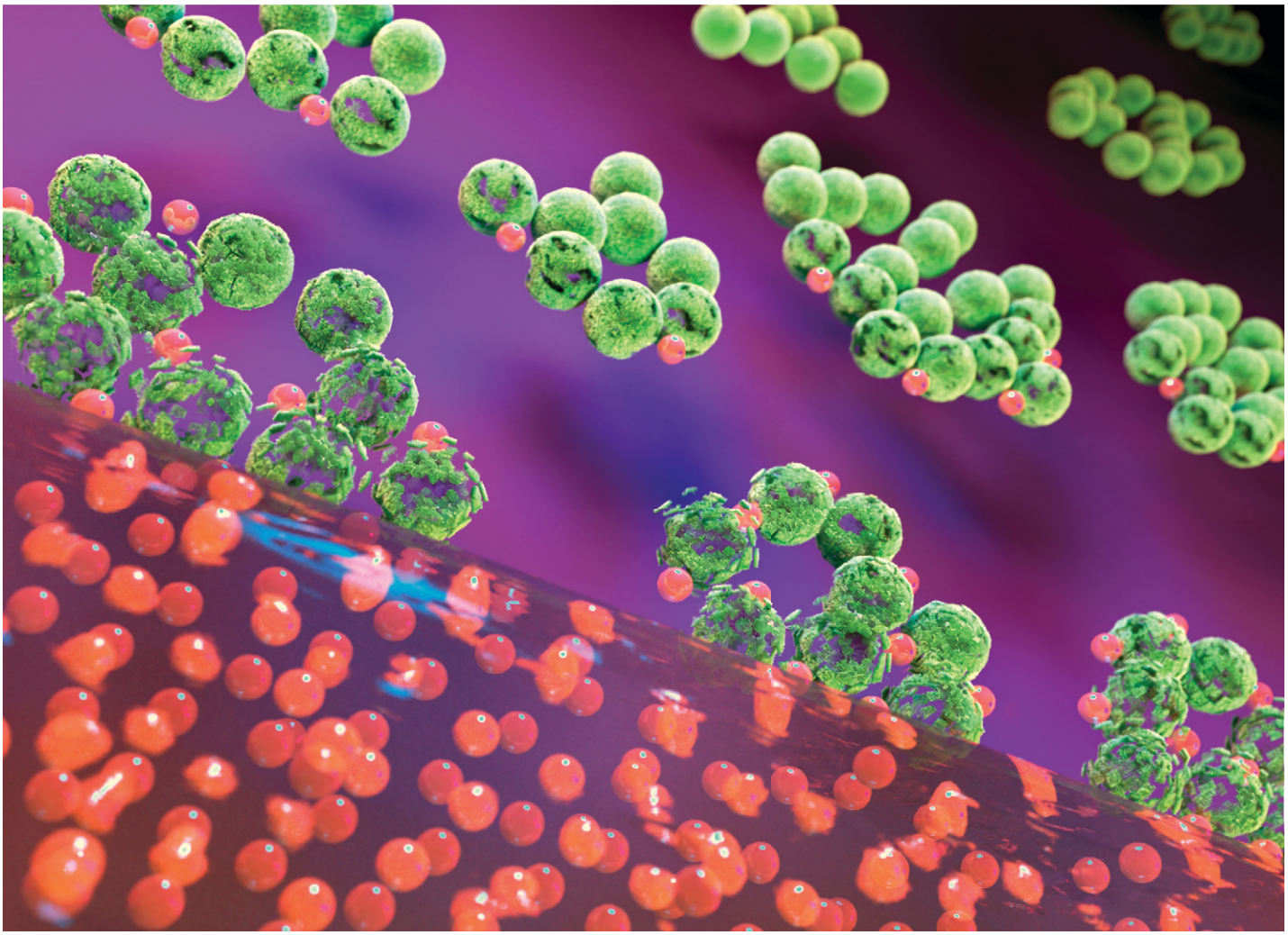

Showcasing research from Professor Kirillov's laboratory, Instituto Superior Técnico, University of Lisbon, Portugal.

Sulfonyldibenzoate coordination polymers as bioactive dopants for polysaccharide films with antibacterial and antibiofilm properties

Biopolymer-Bacteria Interfaces: Where Biopolymers Battle Bacteria. Antimicrobial silver(I) and copper(II) coordination polymers were assembled and used as dopants for hybrid biopolymer films based on agarose or potato starch, which feature varying rates of degradability and silver/copper release. The obtained biopolymer films revealed a remarkable antibacterial and biofilm inhibition activity. This study extends the application of coordination compounds as components of hybrid functional materials with antimicrobial properties and prospective biomedical relevance. An interface of polysaccharide biopolymer and its antibacterial action is shown on the cover.

As featured in:

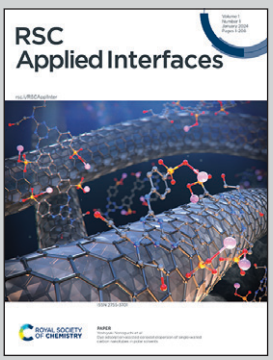

See Alexander M. Kirillov *et al.*, *RSC Appl. Interfaces*, 2024, **1**, 98.

ROYAL SOCIETY OF CHEMISTRY

rsc.li/RSCApplInter

Registered charity number: 207890

RSC Applied Interfaces

ROYAL SOCIETY OF CHEMISTRY

PAPER

View Article Online
View Journal | View Issue

Cite this: *RSC Appl. Interfaces*, 2024, **1**, 98

Sulfonyldibenzoate coordination polymers as bioactive dopants for polysaccharide films with antibacterial and antibiofilm properties†

Tiago A. Fernandes, [ab] Filipa Macedo,[c] Rafaela G. Cabral,[ae] Telma Guiu,[e] Chris H. J. Franco,[a] Paula Jorge,[cd] Ana Catarina Sousa,[ae] Vânia André, [a] Nuno Cerca*[cd] and Alexander M. Kirillov *[a]

This work describes the preparation, characterization, and antimicrobial properties of bioactive silver(I) and copper(II) coordination polymers (bioCPs) and derived biopolymer materials. Two bioCPs, $[Ag_2(\mu_6\text{-sdba})]_n$ (**1**) and $[Cu(\mu_4\text{-sdba})H_2O]_n{\cdot}1.5nH_2O$ (**2**), were assembled from metal salt precursors and 4,4′-sulfonyldibenzoic acid (H_2sdba). Both compounds were used as dopants for preparing hybrid biopolymer films based on agarose (AGR) or potato starch (PS) as model polysaccharide biopolymers with varying rates of degradability and silver/copper release. BioCPs and derived biopolymer films (**1**@$[AGR]_n$, **2**@$[AGR]_n$, **1**@$[PS]_n$, and **2**@$[PS]_n$) with a low loading of dopant (1–5 wt%) show promising antibacterial activity against Gram-positive (*S. aureus* and *S. epidermidis*) and Gram-negative (*E. coli* and *P. aeruginosa*) bacteria. Silver-doped biopolymer films also totally impair the formation of bacterial biofilms, with undetectable biofilm cells in several cases (~7.5 log or 99.99999% inhibition). By reporting new bioCPs and biopolymer films obtained from renewable polysaccharides, this multidisciplinary work extends the application of coordination compounds as components of hybrid functional materials with antimicrobial properties and prospective biomedical relevance.

Received 2nd August 2023,
Accepted 1st November 2023

DOI: 10.1039/d3lf00123g

rsc.li/RSCApplInter

Introduction

Pathogen transmission *via* infected high-touch surfaces and daily items is currently a serious public health problem, especially in hospitals where nosocomial infections are common.[1] Many pathogens present in hospitals show resistance to current antibiotics, posing additional challenges for treating the infections and developing efficient preventive strategies, which include antibacterial materials, coatings, and surfaces.[2,3] Besides, microorganisms are commonly present in the form of biofilms, which are microbial communities enclosed in a protective extracellular matrix that confers an additional barrier to antimicrobial treatment.[4] Thus, there is current demand not just for new antimicrobial compounds but also for bioactive applied materials that can prevent bacterial adhesion and biofilm growth in the first place, resulting in a preventive measure to reduce the number of infections.[5–7]

In this context, bioCPs (bioactive coordination polymers) composed of biocidal metal centers, linkers and/or guest species with antimicrobial action emerged as prospective antibacterial agents.[8–22] Among the metals with antibacterial potential, silver and copper are particularly interesting because of their significant activity and low intrinsic toxicity to human cells.[23–34]

In particular, silver ions, nanoparticles, and coordination compounds feature a number of partially implicit types of antimicrobial mechanisms of action.[32,35–38] The entry of silver(I) species into intracellular protein moieties, notably sulfur-containing proteins and phosphorus-containing deoxyribonucleic acids, is one

[a] *Centro de Química Estrutural, Institute of Molecular Sciences, Departamento de Engenharia Química, Instituto Superior Técnico, Universidade de Lisboa, Av. Rovisco Pais, 1049-001 Lisbon, Portugal. E-mail: kirillov@tecnico.ulisboa.pt*
[b] *Departamento de Ciências e Tecnologia (DCeT), Universidade Aberta, 1000-013 Lisboa, Portugal*
[c] *Centre of Biological Engineering, University of Minho, Campus de Gualtar, 4710-057 Braga, Portugal. E-mail: nunocerca@ceb.uminho.pt*
[d] *LABBELS–Associate Laboratory, Braga/Guimarães, Portugal*
[e] *Departamento de Engenharia Química, ISEL – Instituto Superior de Engenharia de Lisboa, Instituto Politécnico de Lisboa, R. Conselheiro Emídio Navarro, 1, 1959-007 Lisbon, Portugal*

† Electronic supplementary information (ESI) available: Materials and methods; FTIR–ATR spectra (Fig. S1–S4); schematic diagram of $[PS]_n$ and $[PS\text{-}MCC]_n$ biopolymer films (Fig. S5 and S6); TGA data (Fig. S6–S9); water absorption data (Table S1); ICP-OES data for silver or copper ions release from biopolymer samples over time (Fig. S10); crystal data and structure refinement details for **1** (Table S2); additional structural details for **1** and **2** (Table S3, Fig. S12); PXRD patterns (Fig. S11); surface analysis (Fig. S13); mechanical properties of films: tensile strength and elongation (Fig. S14); additional antimicrobial data (Fig. S15 and S16). CCDC 2245521. For ESI and crystallographic data in CIF or other electronic format see DOI: **https://doi.org/10.1039/d3lf00123g**

example. This form of interaction, involving thiol functionalities in important enzymes, contributes to their deactivation, inhibits cell proliferation, and causes cell death.[39–41] Previous research revealed that, upon exposure to Ag^+ species, bacterial DNA loses its capacity to replicate, resulting in alterations in cell membrane structures and the formation of small electron-rich granules containing Ag and S elements.[39–41] Copper coordination compounds also feature several mechanisms of action, including the generation of reactive oxygen species, lipid peroxidation, protein oxidation, and DNA degradation, making them useful in the treatment of viral and microbial infections.[42,43] In addition, the bioactivity of coordination compounds is often superior if compared to parent ligands or inorganic forms of copper.[44,45] In addition to organic and metal–organic compounds, a variety of studies emerged involving biomaterials, including peptide-based materials.[46–48] In the same manner, biopolymers can be a competitive alternative to replace synthetic oil-based plastics and coatings.[49–51] In this context, the development of biopolymer films to create surface coatings that inhibit the adhesion and/or growth of pathogenic bacteria can provide long-term benefits. Such antibacterial coatings or multicomponent mixtures can thus become a viable or complementary alternative to regular surface cleaning.[52–54]

In particular, agarose (AGR) and potato starch (PS) are attractive and low-cost precursors for novel antimicrobial biopolymers.[54–56] AGR polymers have been widely employed in biomedical applications because of their facile manufacture, formability, degradability, tunable water solubility, and non-immunogenic features.[54,57,58] Similarly to AGR, PS is a renewable and sustainable biopolymer, representing one of the most commercially accessible feedstocks for degradable biopolymer films.[59–61]

Considering the above discussion, the main objectives of the present work consisted in: (A) the assembly of silver(I) and copper(II) bioCPs by exploring 4,4′-sulfonyldibenzoic acid (H_2sdba) as a semiflexible dicarboxylate linker; (B) the incorporation of the obtained compounds as bioactive dopants into hybrid biopolymer films based on $[AGR]_n$ or $[PS]_n$; and (C) the evaluation of their antibacterial and biofilm inhibitory activity. The selection of H_2sdba as a main building block was motivated by the following factors: (i) commercial availability, low cost, and presence of two COOH groups with four oxygen sites for potential coordination; and (ii) structural relevance of this sulfonyldibenzoic acid to the sulfadiazine antibiotic and its topical analogue silver(I) sulfadiazine.[62–65] The prepared herein biopolymer films are not intended to be coatings but represent a sort of proof-of-concept materials that may be employed on pre-existing objects or structures, including high-touch surfaces. The present multidisciplinary study not only merges several key research lines on coordination chemistry and applied materials, but it also broadens the antimicrobial use of bioCPs and derived biopolymer films.

Results and discussion

Preparation of bioCPs

The compounds $[Ag_2(\mu_6\text{-sdba})]_n$ (**1**) and $[Cu(\mu_4\text{-sdba})H_2O]_n{\cdot}1.5nH_2O$ (**2**) were self-assembled from an acetonitrile–methanol reaction mixture composed of metal salt precursors (silver(I) nitrate or copper(II) acetate), 4,4′-sulfonyldibenzoic acid (H_2sdba), and aqueous ammonia (Scheme 1). The formulae and structures of the obtained bioCPs were established on the basis of C/H/S analyses, FTIR spectroscopy (Fig. S1–S4†), and crystallography methods, including single-crystal (SCXD) and powder (PXRD) X-ray diffraction (Fig. S11†). The crystal structure of **1** was determined by X-ray diffraction; for structural details, see the ESI.†

Preparation of biopolymer films

Two types of hybrid biopolymer films were fabricated by dispersing low amounts of bioCPs in the biopolymer precursors (AGR or PS with glycerol), followed by polymerization in Petri dishes (Scheme 1, Fig. S4†). Low loadings (1, 2.5, and 5 wt%) of bioCPs were explored, giving origin to thin films of biopolymers (~1 mm thickness, Fig. S5 and S6†), abbreviated as $\mathbf{1}^{(1\%)}$@$[AGR]_n$, $\mathbf{1}^{(2.5\%)}$@$[AGR]_n$, $\mathbf{1}^{(5\%)}$@$[AGR]_n$, $\mathbf{2}^{(1\%)}$@$[AGR]_n$, $\mathbf{2}^{(2.5\%)}$@$[AGR]_n$, and $\mathbf{2}^{(5\%)}$@$[AGR]_n$ (AGR series), as well as $\mathbf{1}^{(5\%)}$@$[PS]_n$ and $\mathbf{2}^{(5\%)}$@$[PS]_n$ (PS series) (Fig. 1). For comparison, the negative control ($[AGR]_n$ and $[PS]_n$) and the positive control samples ($AgNO_3{}^{(1\%)}$@$[AGR]_n$, $AgNO_3{}^{(2.5\%)}$@$[AGR]_n$, $AgNO_3{}^{(5\%)}$@$[AGR]_n$, $AgNO_3{}^{(1\%)}$@$[PS]_n$, $AgNO_3{}^{(2.5\%)}$@$[PS]_n$, $AgNO_3{}^{(5\%)}$@$[PS]_n$, $Cu_2(OAc)_4{}^{(1\%)}$@$[AGR]_n$, $Cu_2(OAc)_4{}^{(2.5\%)}$@$[AGR]_n$, $Cu_2(OAc)_4{}^{(5\%)}$@$[AGR]_n$, $Cu_2(OAc)_4{}^{(1\%)}$@$[PS]_n$, $Cu_2(OAc)_4{}^{(2.5\%)}$@$[PS]_n$, and $Cu_2(OAc)_4{}^{(5\%)}$@$[PS]_n$) were also fabricated. Prior to analysis, all the prepared biopolymer films were kept in an oven at 36 °C.

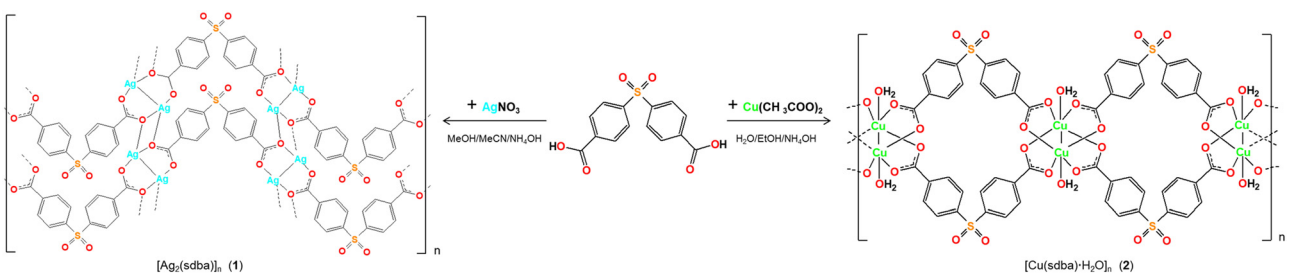

Scheme 1 Synthesis of compounds **1** and **2**.

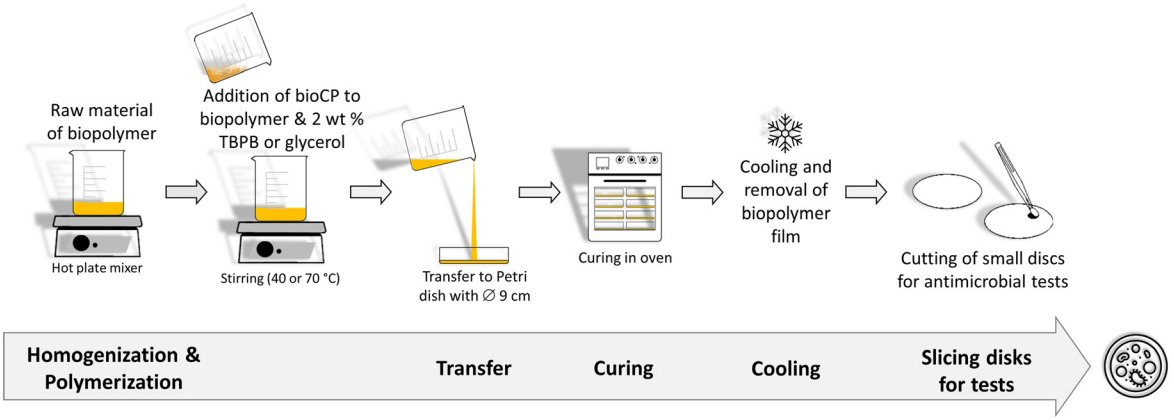

Fig. 1 Preparation of bioCP-doped biopolymer films. TBPB: *tert*-butyl peroxybenzoate.

The obtained biopolymer films were characterized by Fourier transform infrared spectroscopy – attenuated total reflectance (FTIR–ATR) (Fig. S1–S4†), thermogravimetric analysis (TGA) (Fig. S7–S9†), and scanning electron microscopy with energy dispersive X-ray analysis (SEM–EDX). The latter revealed mostly uniform dispersion of bioCPs, although locations with crystalline agglomerates can be observed in some samples. In addition to silver and copper ion release tests, water absorption and polymer film stability in PBS (phosphate buffered saline) were examined (Table S1, Fig. S10†). In fact, AGR-based biopolymer films disaggregated over time in PBS medium (Fig. S11†), disclosing a lower release of Ag(I) ions from **1** if compared to Cu(II) ions from **2**. After 48 h, there was a release of 0.56 mg L^{-1} of Ag^{+} and 2.4 mg L^{-1} of Cu^{2+} for the $[AGR]_n$ films doped with 5% of **1** and **2**, respectively. These metal ion release values correspond to ~1.1% of all silver present in $\mathbf{1}^{(5\%)}$@$[AGR]_n$ and ~12.1% of all copper present in $\mathbf{2}^{(5\%)}$@$[AGR]_n$.

The obtained bioCPs are marginally soluble in water and in the reaction medium during the film formation, thus making difficult their homogeneous distribution in the biopolymer films. It should be mentioned that, in contrast to discrete metal complexes or soluble metal salts, the release of metal ions from films doped with **1** and **2** is significantly slower, which represents an advantage in terms of relative stability and prolonged action as antimicrobial materials.

The use of H_2sdba as a linker for the assembly of **1** and **2** aimed at better understanding the role of metal ions on the observed antibacterial activity. Besides, as a ligand, H_2sdba has not been explored for the synthesis of antimicrobial coordination compounds in spite of structural relevance of this sulfonyldibenzoic acid to sulfadiazine antibiotic,[65] and its topical analogue silver(I) sulfadiazine.[62–64] By applying the same ligand as a main building block for **1** and **2**, 4,4′-sulfonyldibenzoic acid ($\log P$ = 2.66 ± 0.36; $\log P$, octanol–water partition coefficient),[66] it was possible to investigate the importance of the biopolymer matrix and the effect of the metal ion type.

Structural description of bioCPs 1 and 2

Compound **1** belongs to a monoclinic crystal system with $P2_1/m$ space group and adopts a 2D metal–organic network structure (Fig. 2). The asymmetric unit contains one crystallographically independent Ag(I) ion and a half of μ_6-$sdba^{2-}$ ligand, representing a 2 : 1 ratio between silver and dicarboxylate linker. The C–O bond distances of COO^{-} groups are similar (average difference of 0.008 Å), suggesting an electronic conjugation expected after deprotonation; these data are in agreement with the FTIR–ATR analysis (Fig. S1†). The Ag(I) site assumes a slightly distorted seesaw $\{AgO_3Ag^{ii}\}$ geometry, composed of three O atoms ($O1^{ii}$, $O1^{iv}$, and O2) of three μ_6-$sdba^{2-}$ ligands, with the τ_4 (0.32) and τ_4' (0.28) index parameters (Fig. 2b).[67] These τ parameters are defined by the relationship between the two largest angles around the four-coordinate metal centers (α = 151.06(12)° and β = 163.5(2)°) and angle θ, where θ = 109.5°. Values close to 0.43 for τ_4 and 0.24 for τ_4' indicate a seesaw geometry.[61] In addition, the Ag–O bond lengths in **1** are 2.152(5) Å [Ag1–O2], 2.171(5) Å

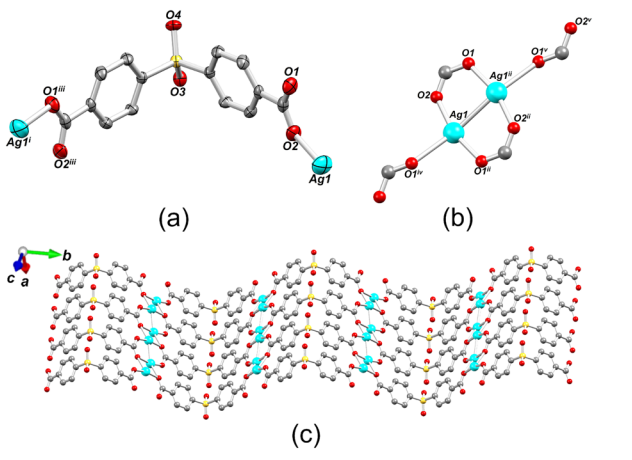

Fig. 2 Structural representations of **1**. (a) Connectivity of μ_6-$sdba^{2-}$ ligand. (b) Coordination environment around Ag1 centers (some atoms are omitted for clarity). Symmetry code: i (–1 – *x*, ½ + *y*, 1 – *z*); ii (–1 – *x*, 1 – *y*, 1 – *z*); iii (*x*, ½ – *y*, *z*); iv (*x*, *y*, 1 + *z*); v (–1 – *x*, 1 – *y*, –*z*). (c) 2D metal–organic layer along the *bc* plane. Ag (cyan), O (red), S (yellow), C (gray).

[Ag1–O1^{i}], and 2.695(7) Å [Ag1–O1^{iv}], which are normal for silver-carboxylate derivatives.[19,68,69] Other selected bonding parameters are displayed in the ESI† (Table S2). The VDP (Voronoi direct polyhedra) for the Ag–O bonds were calculated, showing the following values of solid angle (in %) and area (Å^2): 20.1%/6.7 Å^2 for [Ag1–O2], 20.7%/7.3 Å^2 for [Ag1–O1^{i}], and 12.2%/4.4 Å^2 for [Ag1–O1^{iv}]. The observed difference between these values is an indication that compound **1** is less stable along the *c* axis and begins to degrade in this direction. This observation is in agreement with the observed powder X-ray diffraction data (Fig. S11a and S12†), showing that the (020) crystal face is the most pronounced and, possibly, Ag(I) ions are more exposed in this direction. The Ag···Ag contact of 2.8521(17) Å is smaller than the sum of van der Waals radii of Ag(I) (3.44 Å), suggesting the presence of argentophilic interactions,[70] which are typical for silver(I) coordination polymers.[71–75]

The crystal structure of **1** consists of disilver(I) units linked by carboxylate moieties to create the 1D chain motifs, which are further joined into a zigzag 2D network in the *bc* plane. The 2D sheets are stacked as a "sandwich framework" along the diagonal of the crystallographic ac plane (Fig. 3a). It is possible to observe that the dihedral angle between the two aromatic rings of μ_6-sdba^{2-} is 102.3(4)°. The topological description of the coordination network of **1** was performed using the ToposPro software.[76] The disilver(I) units and μ_6-sdba^{2-} linkers were considered in the network simplification as the 4-connected and topologically equal nodes (Fig. 2c), resulting in a mononodal **sql** [Shubnikov tetragonal plane net] network with a point symbol of $\{4^4{\cdot}6^2\}$.

The structure of $[Cu(\mu_4\text{-sdba})H_2O]_n{\cdot}1.5nH_2O$ (**2**) belongs to a monoclinic space group *C*2/*m* and features a 1D coordination polymer chain with a 2C1 topology (Fig. 4). The Cu(II) atoms in the dicopper(II) unit have a distorted $\{CuO_5\}$ square-pyramidal geometry formed by four bridging carboxylate oxygen atoms and one terminal H_2O ligand (Cu–O 1.961(3)–2.959(3) Å), which produces paddlewheel Cu_2 units. For additional details, consult CCDC 960064.[77]

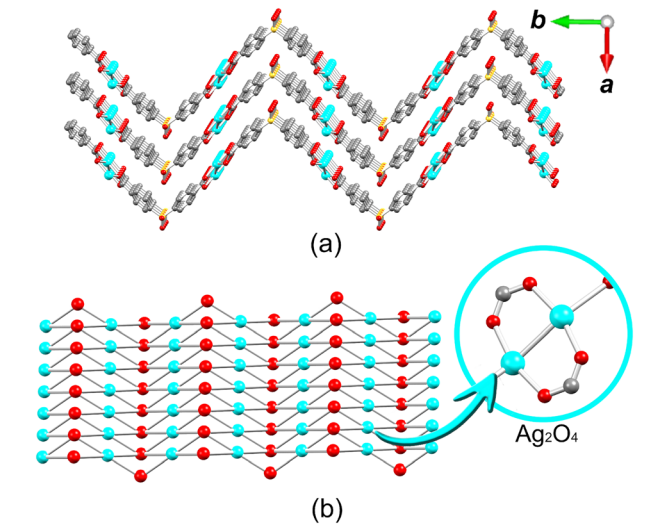

Fig. 3 Packing and topological representations of **1**. (a) Zigzag 2D layers of **1** ("sandwich") along the *ac* plane; color codes are those of Fig. 2. (b) Topological representation of simplified **sql** net in **1**; Ag2 units (cyan balls), centroids of μ_6-sdba^{2-} (red balls).

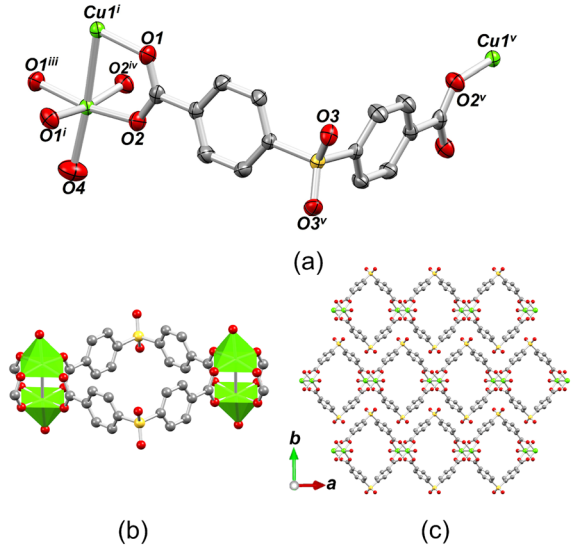

Fig. 4 Structural representations of **2**. (a) Coordination of μ_4-sdba^{2-} ligand to copper centers. Symmetry codes: i (–1 – *x*, *y*, 2 – *z*); iii (1 – *x*, 1 – *y*, 2 – *z*); iv (*x*, 1 – *y*, *z*); v (–*x*, *y*, –*z*). (b) Representation of paddlewheel Cu_2 units. (c) 1D coordination polymer chains along the *a* axis (CCDC code: VIZRAZ).

Powder X-ray diffraction analysis

The experimental patterns were compared to simulated ones derived from the single crystal data. The diffraction peaks confirm the crystal structures of both compounds with good crystallinity and phase purity (Fig. S11, ESI†). The average crystallite sizes for **1** (97 ± 28 nm) and **2** (52 ± 19 nm) were obtained using the Scherrer equation ($D_{hkl} = 0.94\lambda/\beta \times \cos\theta$) based on the peaks broadening analysis for (020) and (040) peaks for **1** and (020), (110), (111), and (221) peaks for **2**,[78,79] which were adjusted to spherical geometry. The detailed microstructures of the compounds were studied more extensively by SEM methods, demonstrating particle aggregation resulting in the aggregates of ~10 μm for both compounds **1** and **2**.

Morphological characterization of biopolymer films

The bioCP-doped $[AGR]_n$ and $[PS]_n$ biopolymer films were examined by SEM–EDX (Fig. 5 and S13†) to evaluate their morphology and incorporation of **1** or **2** into the films. The two films, $[AGR]_n$ and $[PS]_n$, have distinct morphologies as seen in Fig. 5a and b. The surface of the $[AGR]_n$ films is smoother and uniform when compared to that of $[PS]_n$. The $[PS]_n$ matrices showed a sludgy surface with inhomogeneous granules (Fig. 5b).[59] Fig. 5d and e represent the surfaces of the two different matrices doped with compound **1**. The dopants contribute to significantly different morphologies on

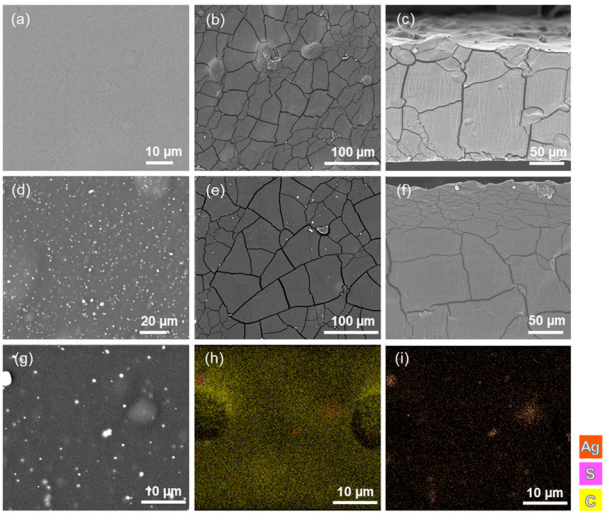

Fig. 5 Morphology characterization using SEM–EDX. SEM images of a) $[AGR]_n$ film; b) $[PS]_n$ film; c) cross section of $[PS]_n$ film; d) $\mathbf{1}^{(5\%)}$@$[AGR]_n$ where CPs particles can be seen throughout at surface of the material; e) $\mathbf{1}^{(5\%)}$@$[PS]_n$; f) cross section of $\mathbf{1}^{(5\%)}$@$[PS]_n$; g) $\mathbf{1}^{(5\%)}$@$[AGR]_n$ with h) an EDX analysis of Ag, C, and S distribution and i) the same section with silver distribution. Images were obtained at various magnifications: g), h), and i) 2000×; a) 1200×; d) 500×; b) and e) 200×; c), f) 160×.

the surface of $[AGR]_n$ films, featuring the agglomerates of bioCPs across the surface (Fig. 5e and S13e–i†). Changes in the surfaces of doped $[PS]_n$ films were blurred (Fig. S13g and k†). It should also be noted that morphological fissures may be seen in both the top view and cross section images (Fig. 5b, c, e and f). These fissures indicate that the material has undergone some dehydration, which can occur as a consequence of film storage at 36 °C.

Both materials were then evaluated by SEM–EDX using silver or copper probes for determining the distribution of Ag or Cu (Fig. 5h, i and S13m–p†). The metal mapping images of the $\mathbf{1}^{(5\%)}$@$[AGR]_n$ and $\mathbf{2}^{(5\%)}$@$[AGR]_n$ films show that silver or copper were barely present on the surface of coupons, as was found for all doped films and on both sides. The surface was primarily composed of carbon and oxygen atoms, with just a few accumulations of silver or copper. When these accumulations emerged, they were accompanied with the presence of sulfur from the sulfonyldibenzoate ligands (Fig. 5h and i). The same was observed for $\mathbf{2}^{(5\%)}$@$[PS]_n$ (Fig. S13o and p†). When examining the full sample coupon, any potential variation in the distribution of Ag or Cu was minimal, as further confirmed by excellent repeatability of biological assays for doped films that were performed in triplicate. Given that both doped materials include morphological fissures, the mechanical properties of the films were evaluated, as well as their stability in the presence of water (Table S1, Fig. S10†).

Mechanical properties

Mechanical properties, such as tensile strength and elongation, were also evaluated for a freshly prepared $[AGR]_n$ and $[PS]_n$ films with and without dopants. In particular, tensile strength values for agarose films (10–13 Mpa) are higher than those of potato starch biopolymers (1–2 Mpa), indicating a more robust character of the former (Fig. S14†). In terms of elongation, the results show that potato starch films are significantly more elastic than agarose films, with a much higher flexibility and extension before rupture. The integration of dopants (up to 5%) into agarose films results in no significant differences in the studied mechanical properties (Fig. S14†).

Thermogravimetric analysis

The thermal stability of bioCP-doped and undoped $[AGR]_n$ and $[PS]_n$ films was investigated by TGA under nitrogen flow (Fig. S7 and S8, ESI†). For $[AGR]_n$, $\mathbf{1}^{(5\%)}$@$[AGR]_n$, and $\mathbf{2}^{(5\%)}$@$[AGR]_n$ films, TGA curves exhibited the same pattern (Fig. S7†). The first mass loss of ~18% was observed until 120 °C, which is primarily due to water release. As the temperature increased from 120 to 260 °C, no changes were detected. A drastic ~44% weight loss was observed for all samples in the range of 260–350 °C. The remaining ~38% of mass was gradually lost from 350 to 800 °C. At this temperature window, three thermograms were slightly different given the presence of dopants. For $[PS]_n$, $\mathbf{1}^{(5\%)}$@$[PS]_n$, and $\mathbf{2}^{(5\%)}$@$[PS]_n$, the TGA plots (Fig. S8†) also followed the same trend. However, $\mathbf{2}^{(5\%)}$@$[PS]_n$ revealed a slight delay in the beginning of the main weight loss effect, wherein ~75% of mass was lost. For $[PS]_n$ and $\mathbf{1}^{(5\%)}$@$[PS]_n$, this occurred in the 150–350 °C range, while for $\mathbf{2}^{(5\%)}$@$[PS]_n$, the interval was shifted to higher temperatures by ~50 °C. The thermal stability of both $[AGR]_n$ and $[PS]_n$ films had little change upon the incorporation of **1** or **2** when compared to the corresponding control films (Fig. S7–S9, ESI†).

Antibacterial activity

Agarose (AGR) and potato starch (PS) biopolymer films were tested against different bacterial species at varying concentrations of dopant, namely 1%, 2.5%, and 5% (m/m). Concerning the doped agarose films, **1**@$[AGR]_n$ and $AgNO_3$@$[AGR]_n$ exhibited bacterial growth inhibition against all strains tested (Fig. 6), in contrast to **2**@$[AGR]_n$, which only showed minor antibacterial properties against *E. coli* (Fig. 6a). In general, the antibacterial activity was dependent on dopant concentration. In addition, **1**@$[AGR]_n$ demonstrated higher efficacy when compared to $AgNO_3$@$[AGR]_n$ in three out of four bacterial species (Fig. 6b–d), which can be beneficial when applied in real-life, since bio-inspired coordination polymers (bioCPs) are more stable when compared to metal salts. The antibacterial activity of the control $[AGR]_n$ and H_2sdba@$[AGR]_n$ films was nonexistent, with the exception for *S. epidermidis*, for which a small growth inhibition hallo was observed (Fig. 6d). As such, all minimum inhibition radii for this species were corrected with the $[AGR]_n$ average value. Despite these observations, agarose and H_2sdba in powder form (bulk material) did not demonstrate antibacterial properties (Fig.

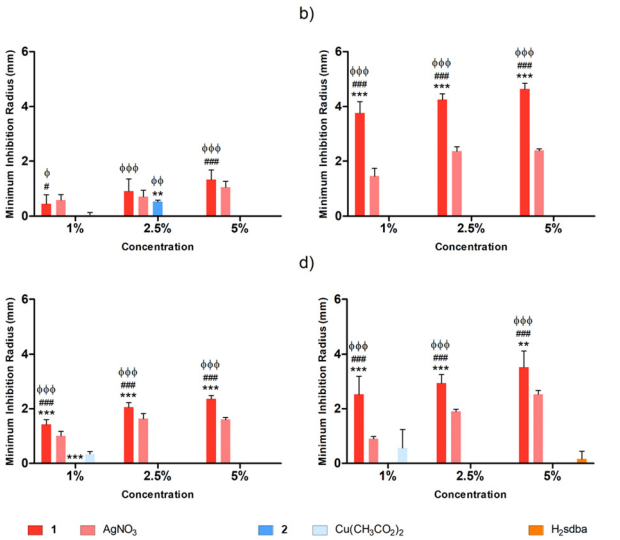

Fig. 6 Normalized antibacterial activity of AGR biopolymer films doped with different concentrations (1%, 2.5%, and 5%, m/m) of **1**, **2**, $AgNO_3$ (silver control), $Cu(OAc)_2$ (copper control), and H_2sdba (organic ligand control) against Gram-negative *E. coli* ATCC 25922 (a) and *P. aeruginosa* PA14 (b) and Gram-positive *S. aureus* ATCC 25923 (c) and *S. epidermidis* RP62A (d) bacterial strains. Significant statistical differences are indicated for the data pairs: **1** and **2** *vs.* $AgNO_3$ and $Cu(OAc)_2$, respectively (*); **1** *vs.* **2** (#); **1** and **2** *vs.* H_2sdba (ϕ). Significance output: $P < 0.05$ (*), $P < 0.01$ (**), $P < 0.001$ (***).

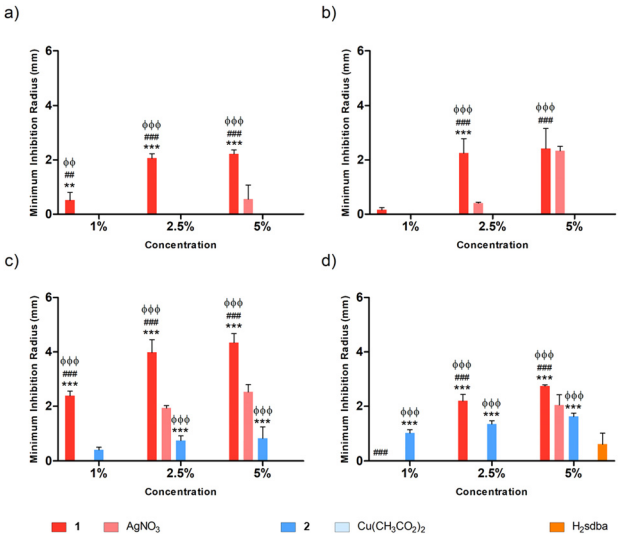

Fig. 7 Normalized antibacterial activity of $[PS]_n$ biopolymer films doped with different concentrations (1%, 2.5%, and 5%, m/m) of **1**, **2**, $AgNO_3$ (silver control), $Cu(OAc)_2$ (copper control), and H_2sdba (organic ligand control) against Gram-negative *E. coli* ATCC 25922 (a) and *P. aeruginosa* PA14 (b) and Gram-positive *S. aureus* ATCC 25923 (c) and *S. epidermidis* RP62A (d) bacterial strains. Significant statistical differences are indicated for the data pairs: **1** and **2** *vs.* $AgNO_3$ and $Cu(OAc)_2$, respectively (*); **1** *vs.* **2** (#); **1** and **2** *vs.* H_2sdba (ϕ). Significance output: $P < 0.05$ (*), $P < 0.01$ (**), $P < 0.001$ (***).

S15†). This distinct result may be due to the formation of agarose nanoparticles with antibacterial activity during the thermal treatment to form $[AGR]_n$ biopolymer films.[80,81] In addition, coordination complexes containing *p*-sulfobenzoic acid are known to be antibacterial.[82] So, the H_2sdba ligand might undergo disaggregation in the medium, generating *p*-sulbobenzoic acid, which has a modest antibacterial activity and may thus justify a minor halo of inhibition (Fig. S15†).

Concerning the doped $[PS]_n$ biopolymer films and in accordance with the previous results about $[AGR]_n$, only **1**@$[PS]_n$ demonstrated bacterial growth inhibition against all bacteria tested (Fig. 7), although in less extent than **1**@$[AGR]_n$ for *P. aeruginosa* (Fig. 6b *vs.* 7b) and *S. epidermidis* (Fig. 6d *vs.* 7d), but better for *E. coli* (Fig. 6a *vs.* 7a) and *S. aureus* (Fig. 6c *vs.* 7c). $AgNO_3$@$[PS]_n$ showed overall reduced antibacterial activity compared to **1**@$[PS]_n$ and also to $AgNO_3$@$[AGR]_n$, with action only at the highest concentrations and virtually no action against *E. coli* (Fig. 7a and S16†). In turn, **2**@$[PS]_n$ films exhibited antibacterial activity against both Gram-positive bacteria, in contrast with the results for **2**@$[AGR]_n$ that showed virtually no activity, which can indicate that the $[PS]_n$ matrix is better at releasing **2** than $[AGR]_n$. Also, while the activity of **1** seems independent of the bacterial Gram-classification both in $[AGR]_n$ and in $[PS]_n$ films (Fig. 6 and 7), **2** is active only against Gram-positive bacteria in $[PS]_n$. In turn, $Cu(OAc)_2$@$[PS]_n$ revealed no antibacterial activity, once again showing the advantages of bioCPs. Similarly to previous results, the antibacterial activity was concentration dependent.[83]

Biofilm inhibition activity

Based on the previous results, the most promising doped films from each matrix type were further tested for their ability to prevent biofilm formation on their surface. Specifically, $\mathbf{1}^{(5\%)}$@$[AGR]_n$ and $\mathbf{1}^{(5\%)}$@$[PS]_n$, along with the corresponding controls, were incubated with four bacterial species and the adhered bacteria were quantified after 24 h. Both $\mathbf{1}^{(5\%)}$@$[AGR]_n$ and $\mathbf{1}^{(5\%)}$@$[PS]_n$ were able to prevent biofilm formation on their surface in variable degrees depending on the species and the matrix type (Fig. 8). This activity was significantly higher than that of both controls,

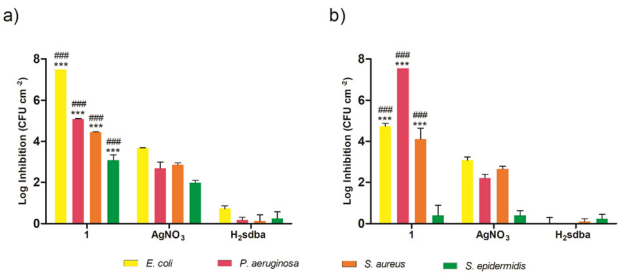

Fig. 8 Normalized biofilm inhibition activity of $[AGR]_n$ (a) and $[PS]_n$ (b) biopolymer films doped with 5% (m/m) of **1**, $AgNO_3$ (silver control), and H_2sdba (organic ligand control) against Gram-negative *E. coli* ATCC 25922 and *P. aeruginosa* PA14 and Gram-positive *S. aureus* ATCC 25923 and *S. epidermidis* RP62A bacterial strains. Results are depicted as log reductions compared to the control non-doped matrix. Significant statistical differences are indicated for the data pairs: **1** *vs.* $AgNO_3$ (*); **1** *vs.* H_2sdba (#). Significance output: $P < 0.05$ (*), $P < 0.01$ (**), $P < 0.001$ (***).

except for $\mathbf{1}^{(5\%)}$@$[PS]_n$ against *S. epidermidis* (Fig. 8b). Overall, biofilm inhibition was higher for Gram-negative species than for Gram-positive ones, with the most affected species being *E. coli*, when using $\mathbf{1}^{(5\%)}$@$[AGR]_n$ (Fig. 8a), and *P. aeruginosa*, when using $\mathbf{1}^{(5\%)}$@$[PS]_n$ (Fig. 8b). In fact, culturable biofilm cells were undetectable (below the detection limit of 7.5 log) for these two species in some assays. Given its wider-spectrum activity and effectiveness, $\mathbf{1}^{(5\%)}$@$[AGR]_n$ shows great promise as a candidate for coating strategies to prevent infections related with surface contamination.

Experimental section

Synthesis and characterization of 1 and 2

$[Ag_2(\mu_6\text{-sdba})]_n$ (1). In a vial A, methanol (5 mL) and distilled water (1 mL) were added to $AgNO_3$ (0.170 g, 1 mmol), and the mixture was kept stirring for 10 min at 50 °C. In another vial B containing acetonitrile (15 mL) and methanol (5 mL), 4,4′-sulfonyldibenzoic acid (H_2sdba; 0.153 g, 0.5 mmol) and 6.0 mL of aq. NH_4OH (1 M solution, 6 mmol) were added, and the mixture was kept stirring for 10 min at room temperature. Then, the content of the vial A was slowly added to the vial B, and the obtained reaction mixture was kept stirring for 30 min at room temperature, followed by filtration (filter paper). The obtained filtrate was slowly evaporated in a vial exposed to air. Colorless microcrystals (including suitable for X-ray diffraction) appeared in 1 week, which were separated and air-dried to give bioCP **1** in 58% yield relative to silver(I) nitrate. Anal. Calcd. (%) for **1**, $C_{14}H_8Ag_2O_5S$ (**1**): C 32.34, H 1.55, S 6.17; found: C 32.90, H 1.26, S 6.59. FTIR–ATR (cm^{-1}): 1586 m, 1521 s ν_{as}(COO), 1490 w, 1373 s, 1326 m, 1301 s ν_s(COO), 1133 s, 1071 w, 1012 m, 863 s, 840 w, 775 s, 734 w, 724 s, 690 s.

$[Cu(\mu_4\text{-sdba})H_2O]_n \cdot 1.5nH_2O$ (2). Method A. Compound **2** was synthesized by following the procedure described for **1** but using copper(II) acetate, $Cu(OAc)_2$, instead of silver nitrate. Blue crystals (suitable for X-ray diffraction) of **2** were obtained in 38% yield, based on copper(II) acetate. Method B. An alternative synthetic protocol includes the hydrothermal method wherein copper(II) acetate (0.182 g, 1 mmol) and H_2-sdba (0.153 g, 0.5 mmol) in water/acetonitrile mixture (4 mL/4 mL) were heated in a sealed Teflon-coated stainless steel reactor (20 mL volume) at 130 °C for 120 h. The mixture was then slowly cooled down to 25 °C for 24 h, resulting in microcrystals of **2** in 71% yield. PXRD confirmed the crystal structure of 2.70 Anal. Calcd. (%) for 2, $C_{14}H_8O_6SCu(H_2O)_{2.5}$: C 40.73, H 3.17, S 7.77; found: C 40.61, H 2.61, S 7.82. FTIR–ATR (cm^{-1}): 1617 s, 1571 s ν_{as}(COO), 1490 w, 1406 s ν_{as}(SO), 1331 m ν_s(COO), 1304 m, 1296 m, 1170 s, 1140 m, 1100 m, 1017 m, 872 w, 848 w, 780 m, 742 s, 726 s, 698 s.

Synthesis of bioCP-doped $[AGR]_n$ and $[PS]_n$ films

Prior to incorporation into the $[AGR]_n$ and $[PS]_n$-based biopolymer films, CPs **1** and **2** were mechanically grounded to obtain fine powdered solids. The mixture of agarose (0.2 g) and distilled water (20 mL) (1 : 100 mass ratio) was prepared by mixing agarose powder in water at 150 °C for 20 min. Then, compounds **1** or **2** were introduced and the obtained mixtures were ultrasonically treated for 10 min, and afterwards stirred at 100 °C for 5 min until reaching complete homogenization. The mixtures were poured into Petri dishes (0.09 m of diameter) and maintained at room temperature until gelatinization process. The formed gels were removed from the Petri dishes and kept in an oven at 60 °C for polymerization during 24 h. The obtained flexible films were abbreviated as $\mathbf{1}^{(1\%)}$@$[AGR]_n$, $\mathbf{1}^{(2.5\%)}$@$[AGR]_n$, $\mathbf{1}^{(5\%)}$@$[AGR]_n$, $\mathbf{2}^{(1\%)}$@$[PS]_n$, $\mathbf{2}^{(2.5\%)}$@$[AGR]_n$, and $\mathbf{2}^{(5\%)}$@$[AGR]_n$. FTIR–ATR (cm^{-1}): 3350 br, 2950 br–m, 2890 br–m, 1653 m, 1373 s, 1180 s, 1152 s, 1115 w, 1065 vs, 1036 vs, 989 w, 965 m, 930 s, 888 m, 772 w.

For the preparation of $[PS]_n$ based biopolymers, PS (1 g), distilled water (10 mL), and glycerol (0.8 mL) (1 : 10 : 0.8 mass ratio) were mixed together for 3 min at 80 °C before adding glycerol. Then, compounds **1** or **2** were added, and the resulting mixtures were stirred for 15 min at 70 °C until completely homogenized. Following that, the mixes were placed into Petri dishes (0.09 m in diameter) and dried in oven at 50 °C for 24 h to polymerize. The malleable biopolymer films were separated from Petri dishes to give the following biopolymer films: $\mathbf{1}^{(1\%)}$@$[PS]_n$, $\mathbf{1}^{(2.5\%)}$@$[PS]_n$, $\mathbf{1}^{(5\%)}$@$[PS]_n$, $\mathbf{2}^{(1\%)}$@$[PS]_n$, $\mathbf{2}^{(2.5\%)}$@$[PS]_n$, and $\mathbf{2}^{(5\%)}$@$[PS]_n$. For comparative and control studies, $[AGR]_n$ and $AgNO_3{}^{(1\%)}$@$[AGR]_n$, $AgNO_3{}^{(2.5\%)}$@$[AGR]_n$, $AgNO_3{}^{(5\%)}$@$[AGR]_n$, $Cu_2(OAc)_4{}^{(1\%)}$@$[AGR]_n$, $Cu_2(OAc)_4{}^{(2.5\%)}$@$[AGR]_n$, $Cu_2(OAc)_4{}^{(5\%)}$@$[AGR]_n$, as well as $[PS]_n$ and $AgNO_3{}^{(1\%)}$@$[PS]_n$, $AgNO_3{}^{(2.5\%)}$@$[PS]_n$, $AgNO_3{}^{(5\%)}$@$[PS]_n$, $Cu_2(OAc)_4{}^{(1\%)}$@$[PS]_n$, $Cu_2(OAc)_4{}^{(2.5\%)}$@$[PS]_n$, $Cu_2(OAc)_4{}^{(5\%)}$@$[PS]_n$ films were produced in parallel experiments. FTIR–ATR (cm^{-1}): 3300 br, 2936 m, 2886 m, 1647 m, 1456 w, 1420 w, 1340 w, 1151 m, 1106, m, 1078 m, 1017 vs, 999 vs, 925 m, 853 m.

X-ray crystallography

Crystal data for **1** were collected on a Bruker AXS-KAPPA APEX II diffractometer and using MoKα (λ = 0.7107 Å) radiation at 293 K. Standard procedures were applied for data reduction using APEX3 programs.[84] The SAINT[85] and SADABS[86] programs were applied for experimental data reduction and scaling Bragg reflections. The crystal structure was solved by direct methods (SHELXS) and refined by full matrix least-squares refinement on F^2 using SHEXL 2014/7.[87] These two programs are included in the WINGX-Version 2014.1 program package.[88] Non-hydrogen atoms were refined anisotropically. All hydrogen atoms bonded to carbon atoms were inserted in calculated positions and refined isotropically [U_{iso}(H) = 1.2U_{eq}(C) and C–H = 0.95 Å] according to the riding model. Crystallographic data and experimental details of data collection and refinement for **1** with formula: $C_{14}H_8Ag_2O_6S$; Fw = 520; crystal form, color: prism, colorless; crystal size: 0.16 × 0.08 × 0.04 mm; crystal system: monoclinic; space group: $P2_1/m$; a = 5.2438(3) Å, b = 24.1388(15) Å, c = 5.7764(4) Å; β = 114.179 (2)°; Z = 2; V = 667.03(7) $Å^3$; D_c = 2.589 g cm^{-3}; μ(MoKα) = 3.122 mm^{-1};

reflections collected/independent: 19333/1237; R_{int} = 0.036; $R_1{}^a$/w$R_2{}^b$ [$I \geq 2\sigma(I)$] = 0.062/0.125; GOF on F^2 = 1.18. ($^aR_1 = \sum||F_o| - |F_c||/\sum|F_o|$. $^bwR_2 = [\sum[w(F_o{}^2 - F_c{}^2)^2]/\sum[w(F_o{}^2)^2]]^{\frac{1}{2}}$). Crystallographic data of compound **1** was deposited within the Cambridge Crystallographic Data Centre (CCDC 2245521).

The powder X-ray diffraction data were obtained using a D8 Advance diffractometer with CuKα (λ = 1.54056 Å), Ni filter and LynxEye linear detector. The diffractograms were collected in the 2θ angular range from 5 to 45°, with a step size of 0.02° and counting time ranging from 0.5 to 1 s per step.

Antibacterial and biofilm inhibition activity

The antibacterial properties of the biopolymer films doped with **1** and **2** were assessed in a soft agar overlay assay. Two Gram-positive (*Staphylococcus aureus* ATCC 25923 and *Staphylococcus epidermidis* RP62A) and two Gram-negative (*Escherichia coli* ATCC 25922 and *Pseudomonas aeruginosa* PA14) bacterial strains were grown overnight in cation adjusted Mueller–Hinton broth (MHB) and were then transferred to soft Mueller–Hinton agar (MHA) (0.5% agar) at a final concentration of 1×10^6 CFU mL^{-1}. Afterwards, 3 mL of the inoculated soft MHA was placed on top of 10 mL of solidified hard MHA (1.7% agar) on a 9 cm diameter Petri dish. The doped film samples were placed on top of the soft MHA and incubated at 37 °C aerobically for 20 h. The antibacterial activity was analyzed by measuring the minimum growth inhibition radius of the formed halos (photographs taken in a Bio-Red ChemicDoc Imager, Bio-Rad Laboratories, Inc., California, USA; halo measures taken with the image editing software GIMP).[89]

For the biofilm inhibition assays, the same bacterial strains were grown in the presence of the films to test for bacterial attachment and biofilm formation.[18] Briefly, bacteria grown overnight, as described above, were transferred to fresh MHB medium at a final concentration of 1×10^6 CFU mL^{-1}. The samples and 1 mL of bacterial suspension were placed into 24 well microtiter plates and incubated for 24 h. Afterwards, the grown bacterial suspension consisting of non-adhered bacteria was removed, and the samples were placed in clean wells and washed twice with 0.9% NaCl solution to remove the remaining non-adhered cells. To quantify the adhered bacteria, the bacteria were detached by submerging the samples in 1 mL of 0.9% NaCl solution and submitting them to an ultrasonic bath (220 V, 50/60 Hz) for 15 min, followed by 30 s of vortex. Finally, the detached bacteria were serially diluted in 0.9% NaCl, plated in hard MHA plates, incubated for 20 h, quantified by CFU counting, and presented as the logarithmic reduction of the number of bacteria per cm^2 of biopolymer compared with the control film (only $[AGR]_n$ or $[PS]_n$). The detection limit for this method was 2 log (CFU cm^{-2}).

Conclusions

In this study, 4,4′-sulfonyldibenzoic acid (H_2sdba) was applied as a promising and still little explored linker for the self-assembly of silver(I) and copper(II) coordination polymers. The obtained $[Ag_2(\mu_6\text{-sdba})]_n$ (**1**) and $[Cu(\mu_4\text{-sdba})H_2O]_n{\cdot}1.5nH_2O$ (**2**) bioCPs feature 2D or 1D networks that are based on Ag_2 or Cu_2 units and sulfonyldibenzoate linkers.

The obtained compounds were used as antibacterial dopants to produce hybrid Ag or Cu-doped biopolymer films derived from agarose and potato starch. The antibacterial activity of the films doped with **1** or **2** was superior in comparison to similar samples where $AgNO_3$ or $Cu(OAc)_2$ were applied as dopants. As expected, the biopolymer films containing the silver(I) bioCP **1** were more effective when compared to those loaded with copper(II) based bioCP **2**, with the latter showing some activity only in the $[PS]_n$ films against Gram-positive bacteria. Both $[AGR]_n$ and $[PS]_n$ films containing **1** revealed very promising biofilm inhibition activity, with the wider spectrum being observed for doped $[AGR]_n$. Additionally, undetectable biofilm growth (~7.5 log inhibition compared to controls) was observed for *E. coli* and *P. aeruginosa* in $[AGR]_n$ and $[PS]_n$, respectively. This result is particularly remarkable for prospective use of these biopolymers when the formation of biofilms should be prevented.

One of the concepts explored in this work was the use of two model biopolymers with varied permeability and stability to generate applied materials with higher or lower Ag(I)/Cu(II) release rates, while using the same type of dopant. We believe that the present work contributes to an underexplored biofilm inhibition application of bioCPs and derived functional materials, while also demonstrating that highly efficient antimicrobial biopolymer films can be easily fabricated from inexpensive biobased raw materials such as agarose and potato starch. Further research on the design of new antimicrobial bioCPs and the application of other biopolymer matrices (*e.g.*, alginate) is currently in progress, also aiming at finding potential correlations between the structural characteristics of compounds, the type of biopolymer matrix, and the resulting antimicrobial properties.

Conflicts of interest

There are no conflicts to declare.

Acknowledgements

This study was supported by the Foundation for Science and Technology (FCT) (projects PTDC/QUI-QIN/3898/2020, PTDC/QUI-QIN/29697/2017, UIDP/00100/2020, UIDB/00100/2020, LA/P/0056/2020, and REM2013; contracts under DL No. 57/2016, CEECIND/02725/2018, CEECIND/00283/2018 and CEECIND/00194/2020) as well as ISEL (IPL/2022/3DBioProd_ISEL, and IPL/2021/Naf4Med3D_ISEL). We thank Dr. Ivo M. F. Bragança for studying the mechanical properties.

References

1 G. Suleyman, G. Alangaden and A. C. Bardossy, The Role of Environmental Contamination in the Transmission of Nosocomial Pathogens and Healthcare-Associated Infections, *Curr. Infect. Dis. Rep.*, 2018, **20**, 12.
2 M. H. Kollef, A. Torres, A. F. Shorr, I. Martin-Loeches and S. T. Micek, Nosocomial Infection, *Crit. Care Med.*, 2021, **49**, 169.
3 B. Song, E. Zhang, X. Han, H. Zhu, Y. Shi and Z. Cao, Engineering and Application Perspectives on Designing an Antimicrobial Surface, *ACS Appl. Mater. Interfaces*, 2020, **12**, 21330.
4 P. Jorge, A. P. Magalhães, T. Grainha, D. Alves, A. M. Sousa, S. P. Lopes and M. O. Pereira, Antimicrobial resistance three ways: Healthcare crisis, major concepts and the relevance of biofilms, *FEMS Microbiol. Ecol.*, 2019, **95**, fiz115.
5 A. Friedlander, S. Nir, M. Reches and M. Shemesh, Preventing biofilm formation by dairy-associated bacteria using peptide-coated surfaces, *Front. Microbiol.*, 2019, **10**, 1405.
6 X. Li, B. Wu, H. Chen, K. Nan, Y. Jin, L. Sun and B. Wang, Recent developments in smart antibacterial surfaces to inhibit biofilm formation and bacterial infections, *J. Mater. Chem. B*, 2018, **6**, 4274.
7 J. Sahoo, S. Sarkhel, N. Mukherjee and A. Jaiswal, Nanomaterial-Based Antimicrobial Coating for Biomedical Implants: New Age Solution for Biofilm-Associated Infections, *ACS Omega*, 2022, **7**, 45962.
8 B. H. Neufeld, M. J. Neufeld, A. Lutzke, S. M. Schweickart and M. M. Reynolds, Metal–Organic Framework Material Inhibits Biofilm Formation of Pseudomonas aeruginosa, *Adv. Funct. Mater.*, 2017, **27**, 1702255.
9 R. Li, T. Chen and X. Pan, Metal–Organic-Framework-Based Materials for Antimicrobial Applications, *ACS Nano*, 2021, **15**, 3808.
10 Y. H. Cheung, K. Ma, H. C. van Leeuwen, M. C. Wasson, X. Wang, K. B. Idrees, W. Gong, R. Cao, J. J. Mahle, T. Islamoglu, G. W. Peterson, M. C. de Koning, J. H. Xin and O. K. Farha, Immobilized Regenerable Active Chlorine within a Zirconium-Based MOF Textile Composite to Eliminate Biological and Chemical Threats, *J. Am. Chem. Soc.*, 2021, **143**, 16777.
11 P. L. Wang, L. H. Xie, E. A. Joseph, J. R. Li, X. O. Su and H. C. Zhou, Metal–organic frameworks for food safety, *Chem. Rev.*, 2019, **119**, 10638.
12 G. Wyszogrodzka, B. Marszałek, B. Gil and P. Dorożyński, Metal-organic Frameworks: Mechanisms of Antibacterial Action and Potential Applications, *Drug Discovery Today*, 2016, **21**, 1009.
13 D. Giliopoulos, A. Zamboulis, D. Giannakoudakis, D. Bikiaris and K. Triantafyllidis, Polymer/metal organic framework (MOF) nanocomposites for biomedical applications, *Molecules*, 2020, **25**, 185.
14 S. W. Jaros, A. Krogul-Sobczak, B. Bażanów, M. Florek, D. Poradowski, D. S. Nesterov, U. Śliwińska-Hill, A. M. Kirillov and P. Smoleński, Self-Assembly and Multifaceted Bioactivity of a Silver(I) Quinolinate Coordination Polymer, *Inorg. Chem.*, 2021, **60**, 15435.
15 S. W. Jaros, M. F. C. Guedes Da Silva, J. Król, M. C. Oliveira, P. Smoleński, A. J. L. Pombeiro and A. M. Kirillov, Bioactive Silver-Organic Networks Assembled from 1,3,5-Triaza-7-phosphaadamantane and Flexible Cyclohexanecarboxylate Blocks, *Inorg. Chem.*, 2016, **55**, 1486.
16 S. W. Jaros, M. F. C. Guedes Da Silva, M. Florek, P. Smoleński, A. J. L. Pombeiro and A. M. Kirillov, Silver(I) 1,3,5-Triaza-7-phosphaadamantane Coordination Polymers Driven by Substituted Glutarate and Malonate Building Blocks: Self-Assembly Synthesis, Structural Features, and Antimicrobial Properties, *Inorg. Chem.*, 2016, **55**, 5886.
17 S. W. Jaros, U. K. Komarnicka, A. Kyzioł, B. Pucelik, D. S. Nesterov, A. M. Kirillov and P. Smoleński, Therapeutic Potential of a Water-Soluble Silver-Diclofenac Coordination Polymer on 3D Pancreatic Cancer Spheroids, *J. Med. Chem.*, 2022, **65**, 11100.
18 T. A. Fernandes, I. F. M. Costa, P. Jorge, A. C. Sousa, R. G. Cabral, V. André, N. Cerca and A. M. Kirillov, Hybrid Silver(I)-Doped Soybean Oil and Potato Starch Biopolymer Films to Combat Bacterial Biofilms, *ACS Appl. Mater. Interfaces*, 2022, **14**, 25104.
19 F. Wu, D. He, L. Chen, F. Liu, H. Huang, J. Dai, S. Zhang and J. You, Antibacterial coordination polymer hydrogels composed of silver(i)-PEGylated bisimidazolylbenzyl alcohol, *RSC Adv.*, 2018, **8**, 20829.
20 Y.-M. Wu, P.-C. Zhao, B. Jia, Z. Li, S. Yuan and C.-H. Li, A silver-functionalized metal–organic framework with effective antibacterial activity, *New J. Chem.*, 2022, **46**, 5922.
21 A. K. Das and P. K. Gavel, Low molecular weight self-assembling peptide-based materials for cell culture, antimicrobial, anti-inflammatory, wound healing, anticancer, drug delivery, bioimaging and 3D bioprinting applications, *Soft Matter*, 2020, **16**, 10065.
22 N. Khan, A. Gupta, V. Shivhare, R. Ahuja, M. Varshney, A. Basu and A. DuttKonar, A heterochiral diphenylalanine auxin derivative empowers remarkable mechanical integrity with promising Antiinflammatory and Antimicrobial Performances, *New J. Chem.*, 2022, **46**, 18262.
23 S. L. Abram and K. M. Fromm, Handling (Nano)Silver as Antimicrobial Agent: Therapeutic Window, Dissolution Dynamics, Detection Methods and Molecular Interactions, *Chem. – Eur. J.*, 2020, **26**, 10948.
24 F. Mao, Y. Su, X. Sun, B. Li and P. F. Liu, Cu(I) Metal–Organic Framework Composites with AgCl/Ag Nanoparticles for Irradiation-Enhanced Antibacterial Activity against E. coli, *ACS Omega*, 2023, **8**, 2733.
25 P. Horcajada, R. Gref, T. Baati, P. K. Allan, G. Maurin, P. Couvreur, G. Férey, R. E. Morris and C. Serre, Metal-organic frameworks in biomedicine, *Chem. Rev.*, 2012, **112**, 1232.
26 Z. Wang, Y. Fang, X. Zhou, Z. Li, H. Zhu, F. Du, X. Yuan, Q. Yao and J. Xie, Embedding ultrasmall Ag nanoclusters in Luria-Bertani extract via light irradiation for enhanced antibacterial activity, *Nano Res.*, 2020, **13**, 203.

27 C. Huang, Y. Cai, X. Chen and Y. Ke, Silver-based nanocomposite for fabricating high performance value-added cotton, *Cellulose*, 2022, **29**, 723.
28 A. Arenas-Vivo, G. Amariei, S. Aguado, R. Rosal and P. Horcajada, An Ag-loaded photoactive nano-metal organic framework as a promising biofilm treatment, *Acta Biomater.*, 2019, **97**, 490.
29 S. T. Nishanthi, K. K. Yadav, A. Baruah, K. Vaghasiya, R. K. Verma, A. K. Ganguli and M. Jha, Nanostructured silver decorated hollow silica and their application in the treatment of microbial contaminated water at room temperature, *New J. Chem.*, 2019, **43**, 8993.
30 Y. Zhang, P. Sun, L. Zhang, Z. Wang, F. Wang, K. Dong, Z. Liu, J. Ren and X. Qu, Silver-Infused Porphyrinic Metal–Organic Framework: Surface-Adaptive, On-Demand Nanoplatform for Synergistic Bacteria Killing and Wound Disinfection, *Adv. Funct. Mater.*, 2019, **29**, 1808594.
31 A. Bhargava, V. Pareek, S. R. Choudhury, J. Panwar and S. Karmakar, Superior Bactericidal Efficacy of Fucose-Functionalized Silver Nanoparticles against Pseudomonas aeruginosa PAO1 and Prevention of Its Colonization on Urinary Catheters, *ACS Appl. Mater. Interfaces*, 2018, **10**, 29325.
32 J. Chen, F. Wang, Q. Liu and J. Du, Antibacterial polymeric nanostructures for biomedical applications, *Chem. Commun.*, 2014, **50**, 14482.
33 F. Marchetti, J. Palmucci, C. Pettinari, R. Pettinari, M. Marangoni, S. Ferraro, R. Giovannetti, S. Scuri, I. Grappasonni, M. Cocchioni, F. J. M. Hodar and R. Gunnella, Preparation of Polyethylene Composites Containing Silver(I) Acylpyrazolonato Additives and SAR Investigation of their Antibacterial Activity, *ACS Appl. Mater. Interfaces*, 2016, **8**, 29676.
34 T. A. Fernandes, F. Mendes, A. P. S. Roseiro, I. Santos and M. F. N. N. Carvalho, Insight into the cytotoxicity of polynuclear Cu(I) camphor complexes, *Polyhedron*, 2015, **87**, 215.
35 N. Kircheva, S. Dobrev, V. Nikolova, S. Angelova and T. Dudev, Theoretical Insight into the Phosphate-Targeted Silver's Antibacterial Action: Differentiation between Gram (+) and Gram (−) Bacteria, *Inorg. Chem.*, 2022, **61**, 10089.
36 X. Xie, T. C. Sun, J. Xue, Z. Miao, X. Yan, W. W. Fang, Q. Li, R. Tang, Y. Lu, L. Tang, Z. Zha and T. He, Ag Nanoparticles Cluster with pH-Triggered Reassembly in Targeting Antimicrobial Applications, *Adv. Funct. Mater.*, 2020, **30**, 2000511.
37 H. A. Tran and P. A. Tran, In Situ Coatings of Silver Nanoparticles for Biofilm Treatment in Implant-Retention Surgeries: Antimicrobial Activities in Monoculture and Coculture, *ACS Appl. Mater. Interfaces*, 2021, **13**, 41435.
38 E. Gascón, S. Maisanaba, I. Otal, E. Valero, G. Repetto, P. G. Jones and J. Jiménez, (Amino)cyclophosphazenes as Multisite Ligands for the Synthesis of Antitumoral and Antibacterial Silver(I) Complexes, *Inorg. Chem.*, 2020, **59**, 2464.
39 J. R. Morones, J. L. Elechiguerra, A. Camacho, K. Holt, J. B. Kouri, J. T. Ramírez and M. J. Yacaman, The bactericidal effect of silver nanoparticles, *Nanotechnology*, 2005, **16**, 2346.
40 P. R. More, S. Pandit, A. D. Filippis, G. Franci, I. Mijakovic and M. Galdiero, Silver Nanoparticles: Bactericidal and Mechanistic Approach against Drug Resistant Pathogens, *Microorganisms*, 2023, **11**, 369.
41 Q. L. Feng, J. Wu, G. Q. Chen, F. Z. Cui, T. N. Kim and J. O. Kim, A mechanistic study of the antibacterial effect of silver ions on Escherichia coli and Staphylococcus aureus, *J. Biomed. Mater. Res.*, 2000, **52**, 662.
42 J. Das, S. Ta, N. Salam, S. Das, S. Ghosh and D. Das, Polymeric copper(ii) and dimeric oxovanadium(v) complexes of amide-imine conjugate: bilirubin recognition and green catalysis, *RSC Adv.*, 2023, **13**, 13195.
43 M. K. Lesiów, U. K. Komarnicka, A. Kyzioł, A. Bieńko and P. Pietrzyk, ROS-mediated lipid peroxidation as a result of Cu(II) interaction with FomA protein fragments of F. nucleatum: relevance to colorectal carcinogenesis, *Metallomics*, 2019, **11**, 2066.
44 J. R. J. Sorenson, Copper-complexes in biochemistry and pharmacology, *Prog. Med. Chem.*, 1984, **26**, 437.
45 S. Zehra, S. Tabassum and F. Arjmand, Biochemical pathways of copper complexes: progress over the past 5 years, *Drug Discovery Today*, 2021, **26**, 1086.
46 P. K. Gavel, D. Dev, H. S. Parmar, S. Bhasin and A. K. Das, Investigations of Peptide-Based Biocompatible Injectable Shape-Memory Hydrogels: Differential Biological Effects on Bacterial and Human Blood Cells, *ACS Appl. Mater. Interfaces*, 2018, **10**, 10729.
47 N. Khan, A. Gupta, V. Shivhare, R. Ahuja, A. Basu and A. DuttKonar, Can the stereogenicity in aromatic/non-aromatic residues influence the mechanical integrity, antimicrobial and anti-inflammatory preferences of auxin derivatized hydrogels?, *New J. Chem.*, 2022, **46**, 22393.
48 P. Tiwari, A. Gupta, D. N. Shukla, A. K. Mishra, A. Basu and A. DuttKonar, Chiral Orchestration: A Tool for Fishing Out Tripeptide-Based Mechanoresponsive Supergelators Possessing Anti-Inflammatory and Antimicrobial Properties, *ACS Appl. Bio Mater.*, 2021, **4**, 4119.
49 M. Cruz-Romero and J. P. Kerry, Crop-based biodegradable packaging and its environmental implications, *CAB Rev.: Perspect. Agric. Vet. Sci. Nutr. Nat. Resour.*, 2008, **3**, 1.
50 S. Sid, R. S. Mor, A. Kishore and V. S. Sharanagat, Bio-sourced polymers as alternatives to conventional foodpackaging materials: A review, *Trends Food Sci. Technol.*, 2021, **115**, 87.
51 S. Liu, X. Liu, Y. Ren, P. Wang, Y. Pu, R. Yang, X. Wang, X. Tan, Z. Ye, V. Maurizot and B. Chi, *ACS Appl. Mater. Interfaces*, 2020, **12**, 27876.
52 A. Costa, T. Encarnação, R. Tavares, T. Todo Bom and A. Mateus, Bioplastics: Innovation for Green Transition, *Polymers*, 2023, **15**, 517.
53 A. Banerjee, P. Chowdhury, K. Bauri, B. Saha and P. De, Inhibition and eradication of bacterial biofilm using polymeric materials, *Biomater. Sci.*, 2023, **11**, 11.

54 H. Tabani, M. Alexovič, J. Sabo and M. R. Payán, An overview on the recent applications of agarose as a green biopolymer in micro-extraction-based sample preparation techniques, *Talanta*, 2021, **224**, 121892.
55 Z. Fangfang, B. Xinpeng, G. Wei, G. Wang, Z. Shi and C. Jun, Effects of virgin coconut oil on the physicochemical, morphological and antibacterial properties of potato starch-based biodegradable films, *Int. J. Food Sci. Technol.*, 2020, **55**, 192.
56 X. Hou, H. Wang, Y. Shi and Z. Yue, Recent advances of antibacterial starch-based materials, *Carbohydr. Polym.*, 2023, **302**, 120392.
57 M. A. Salati, J. Khazai, A. M. Tahmuri, A. Samadi, A. Taghizadeh, M. Taghizadeh, P. Zarrintaj, J. D. Ramsey, S. Habibzadeh, F. Seidi, M. R. Saeb and M. Mozafari, Agarose-Based biomaterials: Opportunities and challenges in cartilage tissue engineering, *Polymers*, 2020, **12**, 1150.
58 P. Zarrintaj, B. Bakhshandeh, I. Rezaeian, B. Heshmatian and M. R. Ganjali, A Novel Electroactive Agarose-Aniline pentamer Platform as a Potential Candidate for Neural Tissue Engineering, *Sci. Rep.*, 2017, **7**, 17187.
59 A. H. D. Abdullah, S. Pudjiraharti, M. Karina, O. D. Putri and R. H. Fauziyyah, Potato Starch-based Bioplastics Plasticized with Glycerol, *J. Biol. Sci.*, 2019, **19**, 57.
60 M. M. Altayan, T. al Darouich and F. Karabet, On the Plasticization Process of Potato Starch: Preparation and Characterization, *Food Biophys.*, 2017, **12**, 397–403.
61 G. Coppola, M. T. Gaudio, C. G. Lopresto, V. Calabro, S. Curcio and S. Chakraborty, Bioplastic from Renewable Biomass: A Facile Solution for a Greener Environment, *Earth Syst. Environ.*, 2021, **5**, 231.
62 R. J. White and R. Copper, Silver sulphadiazine: A review of the evidence, *Wounds*, 2005, 51.
63 M. Waqas, A. Nazir, Q. H. Qureshi, R. Masood, T. Hussain, M. Q. Khan and S. Abid, Silver sulfadiazine loaded nanofibers for burn infections, *Int. J. Polym. Mater.*, 2023, **72**, 517.
64 J. L. Tanaka, C. B. Costa-Orlandi, B. S. Burd, G. S. A. Pegorin, T. V. da Silva, N. B. Guerra, M. J. S. Mendes-Giannini, A. M. Fusco-Almeida, R. D. Herculano and N. R. de Barros, Natural rubber dressing loaded with silver sulfadiazine for the treatment of burn wounds infected with Candida spp., *Int. J. Biol. Macromol.*, 2021, **189**, 597.
65 R. A. Azzam, R. E. Elsayed and G. H. Elgemeie, Design, Synthesis, and Antimicrobial Evaluation of a New Series of N-Sulfonamide 2-Pyridones as Dual Inhibitors of DHPS and DHFR Enzymes, *ACS Omega*, 2020, **5**, 10401.
66 ACD/ChemSketch (Freeware) 2021.1.3; ACD/Labs 2021.1.3 (File Version C25E41, Build 123835, 29 Aug 2021); LogP (v.14.50).
67 L. Yang, D. R. Powell and R. P. Houser, Structural variation in copper(i) complexes with pyridylmethylamide ligands: Structural analysis with a new four-coordinate geometry index, τ4, *Dalton Trans.*, 2007, 955.
68 Y. D. Yang, C. C. Fan, B. M. Rambo, H. Y. Gong, L. J. Xu, J. F. Xiang and J. L. Sessler, Multicomponent self-assembled metal-organic [3]rotaxanes, *J. Am. Chem. Soc.*, 2015, **137**, 12966.
69 H. M. Titi and I. Goldberg, Crystal engineering with 1-benzofuran-2,3-dicarboxylic acid: Co-crystals with bipyridyl ligands, discrete complexes and coordination polymers with metal ions, *CrystEngComm*, 2010, **12**, 3914.
70 H. Schmidbaur and A. Schier, Argentophilic interactions, *Angew. Chem., Int. Ed.*, 2015, **54**, 746.
71 L. Dai, W. You, E. Wang, S. Wu, Z. Su, Q. Du, Z. Yi and Y. Fang, Two novel one-dimensional α-keggin-based coordination polymers with argentophilic {Ag3}3+/{Ag4}4+ clusters, *Cryst. Growth Des.*, 2009, **9**, 2110.
72 D. Sun, R. Cao, J. Weng, M. Hong and Y. Liang, A novel luminescent 3D polymer containing silver chains formed by ligand unsupported Ag-Ag interactions and organic spacers, *J. Chem. Soc., Dalton Trans.*, 2002, 291.
73 T. A. Fernandes, I. F. M. Costa, P. Jorge, A. C. Sousa, V. André, N. Cerca and A. M. Kirillov, Silver(I) Coordination Polymers Immobilized into Biopolymer Films for Antimicrobial Applications, *ACS Appl. Mater. Interfaces*, 2021, **13**, 12836.
74 G. Lamming, J. Kolokotroni, T. Harrison, T. J. Penfold, W. Clegg, P. G. Waddell, M. R. Probert and A. Houlton, Structural Diversity and Argentophilic Interactions in One-Dimensional Silver-Based Coordination Polymers, *Cryst. Growth Des.*, 2017, **17**, 5753.
75 L. Mistry, O. El-Zubir, T. Pope, P. G. Waddell, N. Wright, W. A. Hofer, B. R. Horrocks and A. Houlton, Silver-Cytidine Coordination Polymer: Electrical Properties, Modulating Intrachain Ag···Ag Distance, and MOF-Nanosheet Transformation, *Cryst. Growth Des.*, 2021, **21**, 4398.
76 V. A. Blatov, A. P. Shevchenko and D. M. Proserpio, Applied topological analysis of crystal structures with the program package topospro, *Cryst. Growth Des.*, 2014, **14**, 3576.
77 Q. Q. Zhou, R. Q. Miao, D. F. Wang and R. bin Huang, Syntheses, structures and properties of three novel Cu(II) coordination compounds based on 4,4′-oxybisbenzoic acid, *J. Mol. Struct.*, 2020, **1206**, 127688.
78 B. Mirtamizdoust, Sonochemical synthesis of nano lead(II) metal-organic coordination polymer; New precursor for the preparation of nano-materials, *Ultrason. Sonochem.*, 2017, **35**, 263.
79 A. S. Vorokh, Scherrer formula: estimation of error in determining small nanoparticle size, *Nanosyst.: Phys., Chem., Math.*, 2018, 364.
80 R. Satar, S. A. Iizhar, M. Rasool, P. N. Pushparaj and S. A. Ansari, Investigating the antibacterial potential of agarose nanoparticles synthesized by nanoprecipitation technology, *Pol. J. Chem. Technol.*, 2016, **18**, 9.
81 M. Darii, E. S. Beleaev, V. C. Kravtsov, P. Bourosh, Y. Chumakov, J. Hauser, S. Decurtins, S. X. Liu, O. Sultanova and S. G. Baca, Crystalline multicomponent compounds involving hexaammine cobalt(iii) cations, *New J. Chem.*, 2022, **46**, 11404.

82 A. Synowiec, K. Zyła, M. Gniewosz and M. Kieliszek, An effect of positional isomerism of benzoic acid derivatives on antibacterial activity against Escherichia coli, *Open Life Sci.*, 2021, **16**, 594.
83 K. Trusau, P. Jorge, A. C. Sousa, T. A. Fernandes, V. André, M. V. Kirillova, A. Usevich, N. Cerca and A. M. Kirillov, Degradable Copper(II)-Doped Starch-Based Biopolymeric Films with Antibacterial Activity, *RSC Sustainability*, 2023, **1**, 866.
84 Bruker, *APEX3 Ver. 2017.3-0*, Bruker AXS Inc., Madison, Wisconsin, USA, 2017.
85 Bruker, *SAINT+ release 6.22*, Bruker AXS Inc., Madison, Wisconsin, USA, 2005.
86 Bruker, *SADABS*, Bruker AXS Inc., Madison, Wisconsin, USA, 2005.
87 G. M. Sheldrick, SHELXT – Integrated space-group and crystal-structure determination, *Acta Crystallogr., Sect. A: Found. Adv.*, 2015, **71**, 3.
88 L. J. Farrugia, WinGX suite for small-molecule single-crystal crystallography, *J. Appl. Crystallogr.*, 1999, **32**, 837.
89 Image editing software GIMP 2.10.4, 2019.